OPAL Physics Note PN258
10 September 1996

Measurement of the Exclusive τ-Lepton Decay to a Final State with One K^0_S Meson and Three Charged Hadrons

The OPAL Collaboration

Abstract

We describe a measurement of the exclusive branching ratio of the τ lepton to one K^0_S meson accompanied by three charged hadrons, using $Z^0 \to \tau^+\tau^-$ candidates collected with the OPAL detector at LEP during the 1990–1995 running periods. Assuming that two of the three charged hadrons originate from the decay $K^0_S \to \pi^+\pi^-$, we calculate

$$\mathrm{BR}(\tau^- \to K^0_S K^0_S \pi^- \nu_\tau) \;=\; (0.054 \pm 0.030 \pm 0.015)\,\%$$

from a total of 228220 τ candidates, where the first error quoted is statistical and the second is systematic. In this measurement possible contributions from decays with three kaons or additional π^0 mesons are considered to be negligible.

This note describes preliminary OPAL results to be submitted to the XVIII International Symposium on Lepton-Photon Interactions, Hamburg, 28 July - 1 August 1997, and to the International Europhysics Conference on High Energy Physics, Jerusalem, 19-26 August 1997

1 Introduction

Precise measurements of τ lepton branching ratios to final states containing kaons and other mesons have only become possible with the large statistics τ data samples recently available. These measurements are interesting not only as tests of $SU(3)_F$ breaking, but also because the dynamics of the decays are poorly understood. In addition, accurate knowledge of kaon mode branching ratios is necessary to estimate correctly backgrounds in measurements of modes such as $\tau^- \to \pi^- \nu_\tau$ and $\tau^- \to \rho^- \nu_\tau$, which are used to make precise tests of the Standard Model [1].

A measurement of the branching ratio for the mode $\tau^- \to \mathrm{K}^0_S \mathrm{K}^0_S \pi^- \nu_\tau$ is presented in this note using data collected during the 1990–1995 running periods, which amounts to an integrated luminosity of $\sim$174 pb^{-1}. Recent measurements of tau decays to two neutral kaons have also been made by CLEO [2], ALEPH [3], and L3 [4].

2 The OPAL Detector

Before discussing the $\tau^- \to \mathrm{K}^0_S \mathrm{K}^0_S \pi^- \nu_\tau$ selection in more detail, the components of the OPAL detector relevant to this analysis are reviewed. The OPAL detector is described in detail in [5]. The central tracking chambers are contained in a 4 bar pressure vessel and immersed in a 0.435 T axial magnetic field. A 1 m long precision vertex drift chamber with 12 layers of axial wires and 6 layers of small angle (5°) stereo wires extends in radius from 10–21 cm. A large volume (4 m long, 3.7 m diameter) drift chamber (jet-chamber) with 159 layers of axial anode wires surrounds the vertex drift chamber. Positioned outside the jet chamber, z-chambers provide up to six precise measurements of the z-coordinate[1] of charged particles as they leave the tracking system. For the 1991 and subsequent runs a silicon microvertex detector was installed [6] with silicon planes at radii of 6.1 and 7.5 cm.

The jet-chamber allows the full 159 measurements over the polar angle range $|\cos\theta| < 0.73$, while the z-chambers provide measurements to $|\cos\theta| < 0.72$. The momentum in the r-ϕ plane, p_t, is measured in the region $|\cos\theta| < 0.73$ with a resolution of $(\sigma(p_t)/p_t)^2 \sim 0.02^2 + (0.0015 \cdot p_t)^2$ (p_t in GeV). The jet-chamber also provides measurements of the energy loss (dE/dx) of tracks. The dE/dx resolution achieved for tracks with the maximum number of measurements is $\sim$3.5% in multihadronic events and $\sim$3.0% for isolated tracks from $\mathrm{e}^+\mathrm{e}^- \to \mu^+\mu^-$ events [7].

3 Monte Carlo Modelling

Monte Carlo simulation was used in this analysis for the calculation of the selection efficiency for the signal decay mode $\tau^- \to \mathrm{K}^0_S \mathrm{K}^0_S \pi^- \nu_\tau$ as well as background contributions from the $\tau^- \to \mathrm{K}^0_S \pi^- \nu_\tau$, $\tau^- \to \mathrm{K}^0_S \pi^- \pi^0 \nu_\tau$, $\tau^- \to \mathrm{K}^0_S \mathrm{K}^- \pi^0 \nu_\tau$, and $\tau^- \to \mathrm{K}^0_S \mathrm{K}^- \nu_\tau$ channels. Monte Carlo simulation was also used to estimate background from from $\mathrm{e}^+\mathrm{e}^- \to \mathrm{q\bar{q}}$ events. However, a substantial background contribution, misidentified vertices, was estimated from the data.

For the $\tau^- \to \mathrm{K}^0_S \mathrm{X}^- \nu_\tau$ modes, events were generated using KORALZ 4.0 [8] with TAUOLA 2.5 [9], while for $\mathrm{e}^+\mathrm{e}^- \to \mathrm{q\bar{q}}$ background estimation JETSET [10] and HERWIG [11] were used. Generated events were passed through the full OPAL detector simulation [12] and analyzed in the same manner as the data.

[1] In the OPAL coordinate system the z-axis follows the electron beam, the x-axis is directed inwards in the horizontal plane of LEP, and the y-axis is perpendicular to the plane. The radius, r, the polar angle, θ and the azimuthal angle, ϕ, are the usual spherical polar coordinates.

Modelling of the $\tau^- \to K^0_S X^- \nu_\tau$ decays is described in detail in [9]. The $\tau^- \to K^0_S K^0_S \pi^- \nu_\tau$ final state was generated in a modified version of TAUOLA using the model of Finkemeier *et al.* [14] for $\tau^- \to K^0 \bar{K}^0 \pi^- \nu_\tau$ decays. Both vector (ρ') and axial-vector (a_1) contributions were considered with intermediate state decays to $\rho\pi$ or K^*K.

As the dynamics of the decay $\tau^- \to K^0_S K^0_S \pi^- \nu_\tau$ are poorly understood, we have also investigated an alternative model. A Monte Carlo event sample with the default TAUOLA form factors for $\tau^- \to K^0 \bar{K}^0 \pi^- \nu_\tau$ formulated by Decker *et al.* [13] was used to assess possible systematic errors from improper modelling of the $\tau^- \to K^0_S K^0_S \pi^- \nu_\tau$ decays.

In the measurement presented here, the branching ratios of τ decays to final states with three strange particles, or with 2 K^0_S's, a π^- and one or more π^0's, are considered to be negligible as indicated by the small value of $\mathrm{BR}(\tau^- \to K^- K^- K^+ \nu_\tau)$ [15] and by the expected phase-space suppression for decays with four mesons.

4 Event Selection

The selection of $\tau \to K^0_S$ decays is similar to that used in previous OPAL measurements of $\tau \to K^0_S$ branching ratios [16, 17]. In this analysis, however, an additional selection was made to separate decays with a second K^0_S and a charged pion. The selection proceeded in several steps which are outlined here and described in more detail below. First, $Z^0 \to \tau^+\tau^-$ candidates were identified. Tau decays containing at least one two-track secondary vertex with zero charge (V^0's) were identified in these preselected events. The inclusive K^0_S sample, used to study systematic effects in the vertex finding algorithm, comprised a subset of the V^0's with properties consistent with K^0_S mesons. Events with more than one charged track in the hemisphere opposite the K^0_S candidate were rejected in order to reduce contamination from $e^+e^- \to q\bar{q}$ background. Three well measured charged tracks were then required, in addition to the the two from the K^0_S candidate, as a means of eliminating $\tau^- \to K^0_S X^- \nu_\tau$. A set of track quality cuts was imposed to allow for precise $\mathrm{d}E/\mathrm{d}x$ measurements. At least one of the additional tracks was required to be consistent with a track originating from the primary vertex. Events with one or more tracks with $\mathrm{d}E/\mathrm{d}x$ measurements consistent with electrons were removed, as were events with secondary vertices containing four or more charged tracks. These final two requirements reduce contamination from residual photon conversions and decays resulting from hadronic interactions with detector material.

τ–Pair Event Preselection

The preselection of $e^+e^- \to \tau^+\tau^-$ events is almost identical to that used in [18]. However, requirements on the status of detectors not used in the analysis (the end-cap electromagnetic calorimeter, forward detector, and hadron calorimeter) were dropped. Briefly, events were considered to be $e^+e^- \to \tau^+\tau^-$ candidates if they contained two low multiplicity jets consisting of tracks and electromagnetic calorimeter clusters in 35° half-angle cones. The average polar angle of the jets was required to lie within $|\cos\theta_{\mathrm{ave}}| < 0.72$. Backgrounds from $e^+e^- \to e^+e^-$, $e^+e^- \to \mu^+\mu^-$, $e^+e^- \to q\bar{q}$, and $e^+e^- \to (e^+e^-)X$ events were reduced by cuts on the event topology and total visible energy. After these cuts, the total remaining contamination from non τ-pair events was found to be $f^{\mathrm{non}-\tau}_{\mathrm{pre-sel}} = (1.70 \pm 0.12)\%$, estimated from Monte Carlo samples of the backgrounds and corrected with control samples from the data [18, 19].

The total number of τ decays identified by this preselection is 228220. A breakdown by year of the preselected decays is given in table 1.

	1990–1992	1993	1994	1995	Total
Preselected taus	68814	38310	93060	28036	228220
Vertex Candidates	4490	2650	6362	1890	15392
K^0_S Candidates	202	126	282	69	679
5-prong K^0_S Candidates	19	14	27	4	64
$K^0_S K^0_S \pi^-$ Candidates	4	1	3	1	9

Table 1: The numbers of candidates selected by the various stages of the analysis in each year of the data.

K^0_S Identification

Neutral vertex candidates were chosen from intersections of oppositely charged tracks in the $x-y$ plane as described in [16, 17]. These cuts resulted in an efficiency for reconstructing $K^0_S \to \pi^+\pi^-$ decays occurring in the barrel region of the detector of $\sim$58% for K^0_S mesons occurring in τ decays. The number of V^0's identified per year is given in table 1. K^0_S candidates were selected from the identified V^0's using the invariant mass of the vertex reconstructed assuming the tracks to be pions ($M_V(\pi^+\pi^-)$). In order to have the best possible invariant mass resolution, only well reconstructed tracks meeting the following requirements were considered in the mass calculation

- number of z-chamber hits > 3 (out of 6 possible),
- transverse momentum (p_t) between 0.15 and 25.0 GeV.

Backgrounds from photon conversions and multihadronic ($e^+e^- \to q\bar{q}$) events were reduced with mass cuts on

- the invariant mass calculated assuming the tracks to be electrons: $M_V(e^+e^-) > 150$ MeV,
- the invariant mass of all good tracks (assumed to be pions) in the hemisphere defined by the V^0 momentum vector: $M^{K^0_S}_{\mathrm{hemi}} < 2.0$ GeV.

Both the K^0_S peak and the background due to misidentified vertices are well described by the Monte Carlo prediction, although the Monte Carlo is not used to estimate the background from misidentified vertices.

For the purpose of estimating the number of true $K^0_S \to \pi^+\pi^-$ decays in the data sample, signal and sideband regions in $M_V(\pi^+\pi^-)$ were defined as

- Signal Region : 0.460–0.535 GeV
- Lower Sideband : 0.400–0.450 GeV
- Upper Sideband : 0.550–0.700 GeV.

Neutral vertices with $M_V(\pi^+\pi^-)$ lying in the signal region were identified as K^0_S candidates. Those neutral vertex candidates accompanied by 3 well measured charged tracks with a single track in the opposite hemisphere made up the "5-prong K^0_S" sample. The $M_V(\pi^+\pi^-)$ distribution of the identified V^0's in the 5-prong K^0_S sample is shown in figure 1 a) for data and the multihadronic Monte Carlo prediction, and in figures 1 c) and e) for the expectations from signal and $\tau^-\to K^0_S X^-\nu_\tau$ background Monte Carlo samples, respectively.

Numbers of K^0_S candidates per year are given in table 1. The background from misidentified vertices, which amounted to $(22.7\pm5.7)\%$ of the 5-prong K^0_S sample, was estimated using the average number of events per invariant mass bin found in two sideband regions.

Additional Track Requirements

Several cuts were placed on the three charged tracks with momenta in the same hemisphere as the K^0_S momentum to isolate signal events and to ensure a reliable energy loss measurement.

Measurements of energy loss in the jet-chamber are affected by the number of times $\mathrm{d}E/\mathrm{d}x$ is sampled along the track path. Additionally, $\mathrm{d}E/\mathrm{d}x$ predictions depend on an accurate measurement of the track's polar angle. To achieve a good measurement of the track $\mathrm{d}E/\mathrm{d}x$ while still retaining high efficiency for the selection the following $\mathrm{d}E/\mathrm{d}x$ track quality cuts were applied to all additional charged track candidates:

- number of jet-chamber hits usable in the $\mathrm{d}E/\mathrm{d}x$ calculation > 20,
- number of z-chamber hits > 3 (out of 6 possible).

Furthermore, at least one of the three charged tracks was required to be consistent with a track originating from the primary vertex (defined as the average interaction point found over the last $\sim$100 multihadronic events [20]) and had to satisfy:

- number of jet-chamber hits > 80,
- $p_t > 0.15$ GeV,
- the point of closest approach of the track to the primary vertex in the $x-y$ plane: $|d_0| < 0.5$ cm,
- the point of closest approach of the track to the primary vertex in z: $|z_0| < 5.0$ cm,
- the radius of the first hit in the jet-chamber < 75 cm.

Conversion Rejection using dE/dx

The normalized $\mathrm{d}E/\mathrm{d}x$, D_h, for the pion hypothesis for each of the 3 charged tracks accompanying the K^0_S candidate was required to be less than 2 to remove residual conversion electrons, which tend to populate the high tail of the distribution. D_h is defined as :

$$D_h \quad = \quad \frac{\left(\frac{\mathrm{dE}}{\mathrm{dx}}_{\mathrm{meas}}\right) - \left(\frac{\mathrm{dE}}{\mathrm{dx}}^h_{\mathrm{pred}}\right)}{\sigma\left(\frac{\mathrm{dE}}{\mathrm{dx}}^h\right)} \tag{1}$$

where $\frac{\mathrm{dE}}{\mathrm{dx}}_{\mathrm{meas}}$ is the measured $\mathrm{d}E/\mathrm{d}x$ of the track in question calculated using a truncated mean where the highest 30% of the energy loss measurements are discarded [7], $\frac{\mathrm{dE}}{\mathrm{dx}}^h_{\mathrm{pred}}$ is the expected $\mathrm{d}E/\mathrm{d}x$ of that track under particle hypothesis h, and $\sigma(\frac{\mathrm{dE}}{\mathrm{dx}}^h)$ is the expected error on $\mathrm{d}E/\mathrm{d}x$.

The expected mean dE/dx and its error for pions were obtained from $e^+e^- \to q\bar{q}$, $e^+e^- \to e^+e^-$, and $e^+e^- \to \mu^+\mu^-$ data [7]. Note that corrections were not applied to $\frac{dE}{dx}^h_{pred}$ and $\sigma(\frac{dE}{dx}^h)$as in [17]. dE/dx requirements are used only as a means to reject background, not to make differentiations between particle types for exclusive branching ratio measurements. Therefore, the uncorrected quantities were deemed to be of adequate precision for this particular application.

Rejection of Interactions

Events with secondary vertices containing 4 or more charged tracks, identified by a b-tagging algorithm [21], are excluded from the signal sample. In a low-multiplicity environment, these multitrack displaced vertices are often the signature of hadronic interactions between outgoing particles and detector material (e.g. the wall of the central vertex drift chamber). In the b-tagging algorithm used here, secondary vertices were constructed by adding tracks to "seed" vertices formed from tracks with large separation from the primary vertex in the r-ϕ plane. Combinations with vertex fit χ^2 greater than 1% were retained and the process was iterated until no more tracks could be added to the vertex. Only tracks with a significance of separation from the secondary vertex less than the significance of separation from the primary vertex plus an offset of 0.5 were considered as possible candidates to add to the secondary vertex.

The signal sample comprises events in the 5-prong K^0_S sample after rejection of these multitrack secondary vertices. The number of decays passing this "$K^0_S K^0_S \pi^-$" selection is given in table 1.

$\tau^- \to \mathbf{K}^0_S \mathbf{K}^0_S \pi^- \nu_\tau$ Sample

No explicit requirements were made on the three tracks accompanying the identified K^0_S to ensure that one of the two possible oppositely charged combinations was consistent with an additional $K^0_S \to \pi^+\pi^-$ decay. However, CLEO has observed that tau decays to K^0_S and three additional tracks are dominated by $\tau^- \to K^0_S K^0_S \pi^- \nu_\tau$ [2]. Figure 1 b) shows the distribution of the two possible $M(\pi^+\pi^-)$ combinations of additional tracks for the $K^0_S K^0_S \pi^-$ data sample and the multihadronic background prediction while figures 1 d) and f) show the Monte Carlo predictions for $\tau^- \to K^0_S K^0_S \pi^- \nu_\tau$ and $\tau^- \to K^0_S X^- \nu_\tau$ respectively. Although a dearth of statistics precludes making a definitive statement about the presence of a second K^0_S in the data events, an enhancement near the K^0_S mass is clearly visible, consistent with the prediction from the signal Monte Carlo.

The distributions of $M_V(\pi^+\pi^-)$ of the selected vertex versus the two possible $M(\pi^+\pi^-)$ combinations of additional tracks for the $K^0_S K^0_S \pi^-$ sample, the multihadron contamination predicted from Monte Carlo, the $\tau^- \to K^0_S K^0_S \pi^- \nu_\tau$ Monte Carlo sample, and the $\tau^- \to K^0_S X^- \nu_\tau$ background Monte Carlo sample are shown in figures 2, 3, and 4.

5 Signal and Background Estimation

Signal Selection Efficiency

The selection efficiency for $\tau^- \to K^0_S K^0_S \pi^- \nu_\tau$ with respect to the τ-pair preselection was calculated by imposing the selection requirements described in the previous section on a 10,000 event Monte Carlo sample. The efficiency accounts for several effects modeled by the OPAL detector simulation: nuclear interactions, and K^0_S mesons which decay outside the volume of the jet chamber.

The efficiency, $\varepsilon(K^0_S K^0_S \pi^-)$, was measured to be $(4.72\pm0.31)\%$.

Background Estimation

In order to extract the number of $\tau^- \to K^0_S K^0_S \pi^- \nu_\tau$ candidate events from the data sample, several sources of background had to be subtracted. Background contributions coming from the following sources were considered:

- misidentified vertices,
- $e^+e^- \to q\bar{q}$ events,
- $\tau^- \to K^0_S \pi^- \nu_\tau$, $\tau^- \to K^0_S \pi^- \pi^0 \nu_\tau$, $\tau^- \to K^0_S K^- \pi^0 \nu_\tau$, and $\tau^- \to K^0_S K^- \nu_\tau$ decays.

Estimates of the background from misidentified vertices were subtracted from the number of signal events observed in the data. This estimate was made by determining the number of background events in each momentum bin using sidebands (0.400–0.450 GeV and 0.550–0.700 GeV) in the $M_V(\pi^+\pi^-)$ distribution of the vertex tracks. The fraction of the decays in the final event samples arising from misidentified vertices is given in the row labelled as "$f^{\text{mis-ID-V}}$" of table 2.

Contamination from $\tau^- \to K^0_S X^- \nu_\tau$ decays was estimated from Monte Carlo events. These events were subjected to the same selection criteria as the data. The contributing modes $\tau^- \to K^0_S \pi^- \nu_\tau$, $\tau^- \to K^0_S \pi^- \pi^0 \nu_\tau$, $\tau^- \to K^0_S K^- \pi^0 \nu_\tau$, and $\tau^- \to K^0_S K^- \nu_\tau$ were considered separately. The branching fractions used in the calculation were the most recent OPAL measurements[17]:

$$\begin{aligned}
BR(\tau^- \to \bar{K}^0 \pi^- \nu_\tau) &= (1.04 \pm 0.13 \pm 0.09)\ \% \\
BR(\tau^- \to \bar{K}^0 \pi^- \geq 1\pi^0 \nu_\tau) &= (0.48 \pm 0.12 \pm 0.07)\ \% \\
BR(\tau^- \to K^0 K^- \nu_\tau) &= (0.10 \pm 0.07 \pm 0.02)\ \% \\
BR(\tau^- \to K^0 K^- \geq 1\pi^0 \nu_\tau) &= (0.18 \pm 0.09 \pm 0.03)\ \%,
\end{aligned}$$

The fraction of $\tau^- \to K^0_S X^- \nu_\tau$ events predicted in the data samples is given in the row labelled "$f^{\tau^- \to K^0_S X^- \nu_\tau}$" of table 2.

Background from multihadron events was estimated from 3.5 million simulated $e^+e^- \to q\bar{q}$ events generated using the JETSET [10] and the HERWIG [11] Monte Carlos. These events were subjected to the same selection criteria as the data. The fraction of multihadronic events predicted in the data sample is given in the row labelled "f^{MH}" of table 2. To derive these fractions the predicted numbers of multihadronic events surviving the selections were scaled to the number of multihadronic events observed in the data ($\sim$3.7 million).

The Monte Carlo estimate of the level of multihadronic contamination in an inclusive $\tau^- \to K^0_S X^- \nu_\tau$ sample was checked in [17] and found to be in good agreement with the multihadronic background observed in $\tau^+\tau^-$ data.

6 Branching Ratio Calculations

The branching ratio was extracted using the following formula:

$\varepsilon(\mathrm{K}^0_S\mathrm{K}^0_S\pi^-)(\%)$	4.72±0.31
$f^{\mathrm{mis-ID-V}}$ (%)	22.7±5.7
f^{MH} (%)	11.7±11.7
$f^{\tau^-\to\mathrm{K}^0_S\mathrm{X}^-\nu_\tau}$ (%)	4.11±1.11
$f^{\mathrm{bias}}(\tau^-\to\mathrm{K}^0_S\mathrm{K}^0_S\pi^-\nu_\tau)$	0.955±0.008

Table 2: The selection efficiency and bias factor for $\tau^-\to\mathrm{K}^0_S\mathrm{K}^0_S\pi^-\nu_\tau$ and the fractions of decays from misidentified vertices, multihadronic (MH) contamination, and $\tau^-\to\mathrm{K}^0_S\mathrm{X}^-\nu_\tau$.

$$\mathrm{Br}(\tau^-\to\mathrm{K}^0_S\mathrm{K}^0_S\pi^-\nu_\tau) = \frac{\left[\mathrm{N}(\mathrm{K}^0_S\mathrm{K}^0_S\pi^-)-\mathrm{N}^{\mathrm{bgrd}}(\mathrm{K}^0_S\mathrm{K}^0_S\pi^-)\right]}{\mathrm{N}_{\mathrm{pre-sel}}\cdot\left(1-\mathrm{f}^{\mathrm{non}-\tau}_{\mathrm{pre-sel}}\right)\cdot\varepsilon(\mathrm{K}^0_S\mathrm{K}^0_S\pi^-)\cdot f^{\mathrm{bias}}(\tau^-\to\mathrm{K}^0_S\mathrm{K}^0_S\pi^-\nu_\tau)} \tag{2}$$

where

$$\mathrm{N}^{\mathrm{bgrd}}(\mathrm{K}^0_S\mathrm{K}^0_S\pi^-) = (f^{\mathrm{MH}} + f^{\mathrm{mis-ID-V}} + f^{\tau^-\to\mathrm{K}^0_S\mathrm{X}^-\nu_\tau})\cdot\mathrm{N}(\mathrm{K}^0_S\mathrm{K}^0_S\pi^-). \tag{3}$$

In the expressions above, $\mathrm{N}(\mathrm{K}^0_S\mathrm{K}^0_S\pi^-)$ is the number of selected decays, $\mathrm{N}^{\mathrm{pre-sel}}_\tau$ is the number of preselected $\mathrm{e}^+\mathrm{e}^-\to\tau^+\tau^-$ candidates, $\mathrm{N}^{\mathrm{bgrd}}(\mathrm{K}^0_S\mathrm{K}^0_S\pi^-)$ is the expected number of background events, $\varepsilon(\mathrm{K}^0_S\mathrm{K}^0_S\pi^-)$ is the signal selection efficiency, $f^{\mathrm{non}-\tau}_{\mathrm{pre-sel}}$ is the non-τ background fraction in the pre-selection, and f^{X} are the misidentified vertex (mis-ID-V) multihadronic (MH), and $\tau^-\to\mathrm{K}^0_S\mathrm{X}^-\nu_\tau$ decay background fractions. The bias factor, $f^{\mathrm{bias}}(\tau^-\to\mathrm{K}^0_S\mathrm{K}^0_S\pi^-\nu_\tau)$, defined as the ratio of the efficiency of the preselection for finding $\tau^-\to\mathrm{K}^0_S\mathrm{K}^0_S\pi^-\nu_\tau$ events to the average preselection efficiency for all tau decay modes, was estimated using Monte Carlo $\tau^-\to\mathrm{K}^0_S\mathrm{K}^0_S\pi^-\nu_\tau$ events to be $f^{\mathrm{bias}}(\tau^-\to\mathrm{K}^0_S\mathrm{K}^0_S\pi^-\nu_\tau) = 0.955\pm0.008$.

Including only errors from the data statistics from the observed number of signal events and the misidentified vertices background, the branching ratio was measured to be:

$$\mathrm{BR}(\tau^-\to\mathrm{K}^0_S\mathrm{K}^0_S\pi^-\nu_\tau) \quad = \quad (0.054 \pm 0.030)\ \%.$$

7 Systematic Errors

Possible sources of systematic error in this analysis can be broken down into several broad categories. Table 3 summarizes each category's contribution to the total systematic error. Descriptions of how the sizes of these uncertainties were estimated are given below.

In general, systematic uncertainties were studied by considering control samples in the data with similar characteristics to, but larger statistics than, the $\tau^-\to\mathrm{K}^0_S\mathrm{K}^0_S\pi^-\nu_\tau$ data sample.

The first three sources of systematic uncertainty in table 3, the vertex finder efficiency, residual conversions, and efficiency corrections, were taken from [17]. Although the tracking environment is slightly different in this analysis, it is expected that any deviations in the branching ratio measurement due to the presence of a second K^0_S are small relative to the statistical uncertainty.

K^0_S Signal and Background

Systematic errors from the definition of K^0_S candidates and from the method of background estimation using sideband subtraction were studied in the 5-prong K^0_S data sample. To test the sensitivity of the results to possible tails in the $M_V(\pi^+\pi^-)$ distribution not properly modelled in the Monte Carlo, the upper and lower limits of the $M_V(\pi^+\pi^-)$ region used as the K^0_S signal window were varied by ±10 MeV. The rms of the changes of the $\tau^-\to K^0_S K^0_S \pi^- \nu_\tau$ branching ratio measured using the different signal windows from that calculated using the standard window, taken as the systematic error from possible $M_V(\pi^+\pi^-)$ tails, was 6% of the branching ratio.

Biases in the sideband subtraction technique were sought by varying the sideband regions, leading to a relative systematic error of 10%.

Summing these two contributions in quadrature gives the systematic error labelled "K^0_S Signal/Background Estimate" in table 3.

Multihadron Background

The error on the estimate of the multihadronic contamination in the event samples was taken to be 100%, the statistical error on the single $e^+e^-\to q\bar{q}$ Monte Carlo event entering the final selection. The resulting systematic error on the branching ratio was 22.7%. As mentioned before, evidence for multihadron background obtained from studying the opposite hemisphere charge multiplicity in an inclusive $\tau^-\to K^0_S X^- \nu_\tau$ data sample agreed with the $e^+e^-\to q\bar{q}$ Monte Carlo prediction.

Non-τ Background in the Preselection

A small systematic error on the branching ratio arises from the uncertainty on the estimate of the non τ-pair background in the τ-pairs preselection [18]. This error is at the level of 0.1% of the branching ratios.

Monte Carlo Statistics

Limited Monte Carlo statistics are responsible for a 6.5% error in the calculation of the signal efficiency and a 1.1% error due to the uncertainty in the estimate of the $\tau^-\to K^0_S X^- \nu_\tau$ background. These two contributions added in quadrature amount to a systematic error of 6.6%.

Decay Kinematics

Incorrect descriptions of the underlying dynamics of $\tau^-\to K^0_S K^0_S \pi^- \nu_\tau$ decays in the Monte Carlo simulation can cause biases in the estimated efficiencies. We searched for such biases by comparing the signal efficiency calculated from Monte Carlo events for events generated with the default and modified dynamics as described in section 3. From this study, an effect on the branching ratio of 0.6% could not be ruled out. Errors from the modelling of the $\tau^-\to K^0_S X^- \nu_\tau$ background are negligible.

Source	σ(BR)/BR (%)
V–Finder Efficiency	4.1
K^0_S Signal/Background Estimate	11.6
Residual Conversions	4.4
Multihadron Rejection	22.7
Monte Carlo Statistics	6.6
Pre–Selection Background	0.1
Efficiency Corrections	1.4
Decay Kinematics	0.6
$\mathrm{d}E/\mathrm{d}x$	2.0
Total Syst	**27.1**
Statistical	**56.0**

Table 3: Relative systematic errors for the branching ratio measurement. Also shown are the data statistical errors from sideband subtraction.

$\mathrm{d}E/\mathrm{d}x$ Description

Uncertainties from imperfections in the parameterization of $\mathrm{d}E/\mathrm{d}x$ were evaluated by varying the cut on the normalized $\mathrm{d}E/\mathrm{d}x$, assuming the pion hypothesis, from < 1 to < 3. The changes in efficiency relative to the default cut value (< 2) for the 5-prong K^0_S sample were compared to the values of $\Delta\epsilon$ observed for the signal Monte Carlo. This procedure yielded a relative systematic error of 2.0%.

8 Results and Discussion

Including the systematic errors given above, the measurement of the $\tau^- \to K^0_S K^0_S \pi^- \nu_\tau$ branching ratio is:

$$\mathrm{BR}(\tau^- \to K^0_S K^0_S \pi^- \nu_\tau) \quad = \quad (0.054 \pm 0.030 \pm 0.015)\ \%,$$

where the first error quoted is statistical and the second is systematic. In actuality, this measurement should be interpreted as $\mathrm{BR}(\tau^- \to K^0_S 2h^- h^+ \geq 0\pi^0 \nu_\tau)$ where h^- is π^- or K^-. However, the invariant mass distribution of the two opposite sign hadrons (figure 1 b) indicates general consistency with the hypothesis that they come from the decay $K^0_S \to \pi^+\pi^-$, as also observed by CLEO [2]. In addition, the decay $\tau^- \to K^0_S K^0_S K^- \nu_\tau$ is expected to be highly improbable as it is both Cabbibo suppressed and phase-space limited (measurement of the three charged kaon decay mode also indicates that this decay is negligible [15]) while the four meson mode is expected to suffer large phase space suppression.

Although the statistics of the data sample are too small to be able to make any definitive statement about the $\tau^- \to K^0_S K^0_S \pi^- \nu_\tau$ decay dynamics, the result is in reasonable agreement with general trends shown by other experimental measurements [2, 3, 4] and with the most recent phenomenological prediction [14] as shown in table 4.

Exp.	Final State	Measured BR (%)	BR($\tau^-\to K^0\bar{K}^0\pi^-\nu_\tau$) (%)
OPAL	$\tau^-\to \mathbf{K}^0_S\mathbf{K}^0_S\pi^-\nu_\tau$	**0.054 ± 0.030± 0.015**	**0.22±0.12±0.060**
CLEO [2]	$\tau^-\to K^0_S K^0_S\pi^-\nu_\tau$	0.023±0.005±0.003	0.092±0.020±0.012
ALEPH [3]	$\tau^-\to K^0_S K^0_L\pi^-\nu_\tau$	0.26±0.08±0.04	0.52±0.16±0.08
L3 [4]	$\tau^-\to K^0\bar{K}^0\pi^-\nu_\tau$	0.31±0.12±0.04	0.31±0.12±0.04
THEORY [14]	$\tau^-\to K^0_S K^0_S\pi^-\nu_\tau$	0.048	0.20

Table 4: Experimental measurements of the branching ratio BR($\tau^-\to K^0\bar{K}^0\pi^-\nu_\tau$) for different $K^0\bar{K}^0$ combinations and the most recent phenomenological prediction. To facilitate comparisons between measurements, the fraction $K^0_S K^0_S(K^0_L K^0_L)/K^0_S K^0_L$ is taken to be 0.5.

Relating all of these measurements to the $\tau^-\to K^0\bar{K}^0\pi^-\nu_\tau$ branching ratio is not a straightforward task. However, to facilitate comparisons between measurements, the $K^0_S K^0_S(K^0_L K^0_L)/K^0_S K^0_L$ fraction is taken to be 0.5. This fraction depends on the intermediate states through which the decay proceeds. For example, the $K^0_S K^0_S\pi^-$ decay is forbidden by Bose statistics for a $\rho^0\pi^-$ intermediate state. CLEO [2] has estimated that the $K^0_S K^0_S(K^0_L K^0_L)/K^0_S K^0_L$ fraction ranges from 0.25 to 0.50 based on theoretical considerations and experimental measurements of $\tau^-\to K^0K^-\pi^0\nu_\tau$ and $\tau^-\to K^-K^+\pi^-\nu_\tau$.

References

[1] OPAL Collaboration, R.Akers, *et al.*, Z. Phys. **C65** (1995) 1.

[2] CLEO Collaboration, T.E.Coan, *et al.*, Phys. Rev. **D53** (1996) 6037.

[3] ALEPH Collaboration, EPS95 Ref. EPS0448, contribution to the International Europhysics Conference on High Energy Physics, Brussels, 1995.

[4] L3 Collaboration, M.Acciarri, *et al.*, Phys. Lett. **B352** (1995) 487.

[5] OPAL Collaboration, K.Ahmet, *et al.*, Nucl. Instrum. and Methods **A313** (1992) 103.

[6] P.P.Allport, *et al.*, Nucl. Instrum. and Methods **A346** (1994) 476.
P.P.Allport, *et al.*, Nucl. Instrum. and Methods **A324** (1993) 34.

[7] OPAL Collaboration, R.Akers, *et al.*, Z. Phys. **C63** (1994) 181.

[8] S.Jadach, B.F.L.Ward, Z.Wąs, Comput. Phys. Commun. **79** (1994) 503;
KORALZ Version 4.0.

[9] S.Jadach, Z.Wąs, R.Decker, J.H.Kühn, Comput. Phys. Commun. **76** (1993) 361;
TAUOLA Version 2.4. (Version 2.5 includes a simulation of the decay $\tau^-\to K^0_S K^-\nu_\tau$.)

[10] T.Sjöstrand, Comput. Phys. Commun. **82** (1994) 74;
T.Sjöstrand and M.Bengtsson, Comput. Phys. Commun. **43** (1987) 367;
T.Sjöstrand, Comput. Phys. Commun. **39** (1986) 347;
JETSET Versions 7.4 and 7.3 were used.

[11] G.Marchesini and B.R.Weber, Comput. Phys. Commun. **67** (1992) 465;
G.Marchesini and B.R.Weber, Nucl. Phys. **B310** (1988) 461;
HERWIG Version 5.6 was used.

[12] J.Allison, *et al.*, Nucl. Instrum. and Methods **A317** (1992) 47.

[13] R.Decker, E.Mirkes, R.Sauer, and Z.Wąs, Z. Phys. **C58** (1993) 445.

[14] M.Finkemeier and E.Mirkes, Z. Phys. **C69** (1996) 243.

[15] Particle Data Group, R.M.Barnett, *et al.*, Phys. Rev. **D54** (1996) 267.

[16] OPAL Collaboration, R.Akers, *et al.*, Phys. Lett. **B339** (1994) 278.

[17] OPAL Collaboration, OPAL Physics Note PN206, February, 1996.

[18] OPAL Collaboration, G.Alexander, *et al.*, Phys. Lett. **B369** (1996) 244.

[19] OPAL Collaboration, R.Akers, *et al.*, Z. Phys. **C66** (1995) 543.

[20] OPAL Collaboration, P.D.Acton, *et al.*, Z. Phys. **C59** (1993) 183.

[21] OPAL Collaboration, R.Akers, *et al.*, Z. Phys. **C66** (1995) 19.

Figure Captions

Figure 1:
Figures a), c) and e) show the $M_V(\pi^+\pi^-)$ distributions of decays in the 5-prong K^0_S sample without the K^0_S signal mass cut applied. Figures b), d) and f) show the distributions of the two possible $M(\pi^+\pi^-)$ combinations of additional oppositely charged tracks in the $K^0_S K^0_S \pi^-$ sample. Data are plotted in a) and b) as points, with the predicted multihadronic contamination superimposed as the hatched histograms. The Monte Carlo prediction for $\tau^- \to K^0_S K^0_S \pi^- \nu_\tau$ is represented by the histograms in c) and d) while the $\tau^- \to K^0_S X^- \nu_\tau$ background Monte Carlo distributions are given in e) and f).

Figure 2:
The distribution of $M_V(\pi^+\pi^-)$ of the selected vertex versus the two possible $M(\pi^+\pi^-)$ combinations of additional tracks for the $K^0_S K^0_S \pi^-$ sample (unfilled boxes) and the Monte Carlo prediction for multihadronic contamination (hatched boxes). The solid lines denote the K^0_S signal mass cut.

Figure 3:
The distribution of $M_V(\pi^+\pi^-)$ of the selected vertex versus the two possible $M(\pi^+\pi^-)$ combinations of additional tracks for the $\tau^- \to K^0_S K^0_S \pi^- \nu_\tau$ MC sample (arbitrary normalization). The solid lines denote the K^0_S signal mass cut.

Figure 4:
The distribution of $M_V(\pi^+\pi^-)$ of the selected vertex versus the two possible $M(\pi^+\pi^-)$ combinations of additional tracks for the $\tau^- \to K^0_S X^- \nu_\tau$ background MC sample (arbitrary normalization). The solid lines denote the K^0_S signal mass cut.

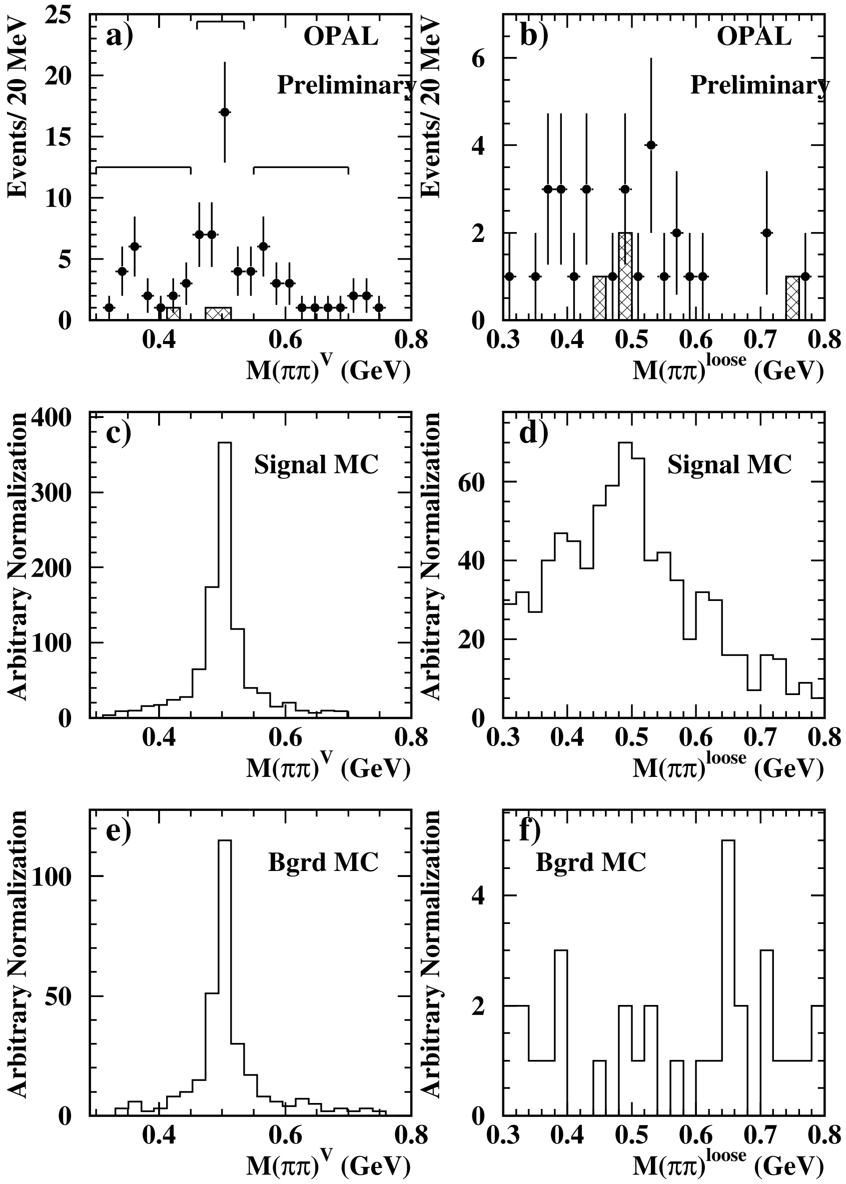
a)
OPAL
Preliminary
Events/ 20 MeV
M(ππ)^V (GeV)
b)
OPAL
Preliminary
Events/ 20 MeV
M(ππ)^loose (GeV)
c)
Signal MC
Arbitrary Normalization
M(ππ)^V (GeV)
d)
Signal MC
Arbitrary Normalization
M(ππ)^loose (GeV)
e)
Bgrd MC
Arbitrary Normalization
M(ππ)^V (GeV)
f)
Bgrd MC
Arbitrary Normalization
M(ππ)^loose (GeV)

Figure 1

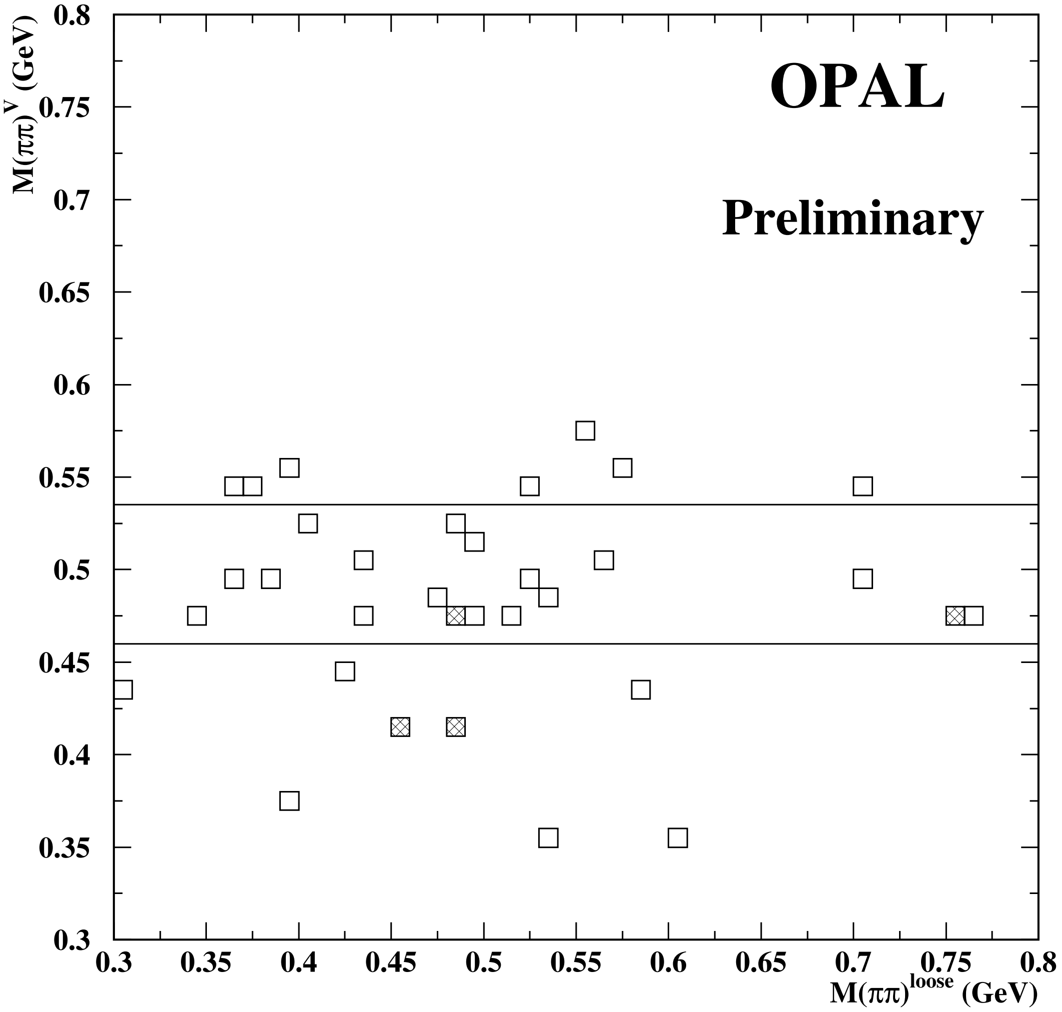
OPAL
Preliminary
M(ππ)^V (GeV)
M(ππ)^loose (GeV)
0.3
0.35
0.4
0.45
0.5
0.55
0.6
0.65
0.7
0.75
0.8

Figure 2

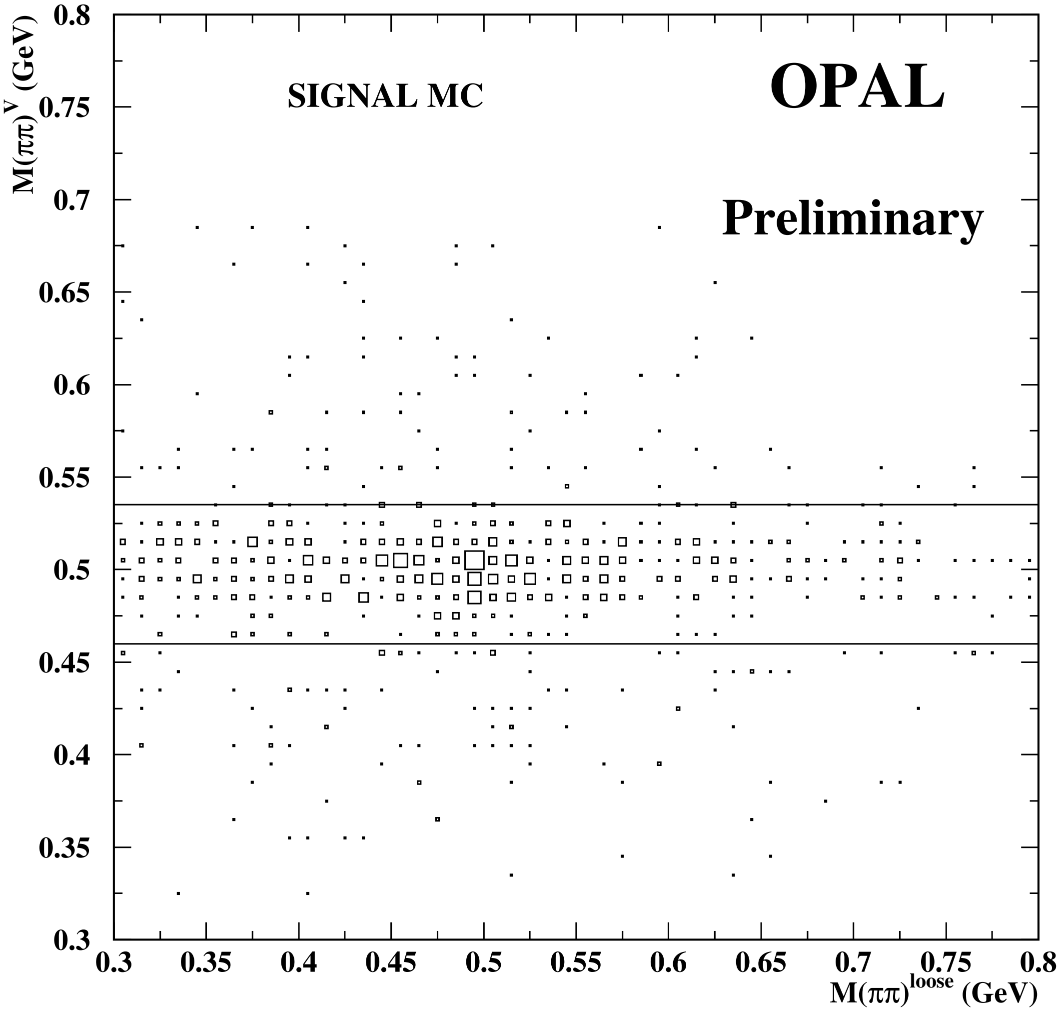
SIGNAL MC
OPAL
Preliminary
M(ππ)^V (GeV)
M(ππ)^loose (GeV)
0.3
0.35
0.4
0.45
0.5
0.55
0.6
0.65
0.7
0.75
0.8

Figure 3

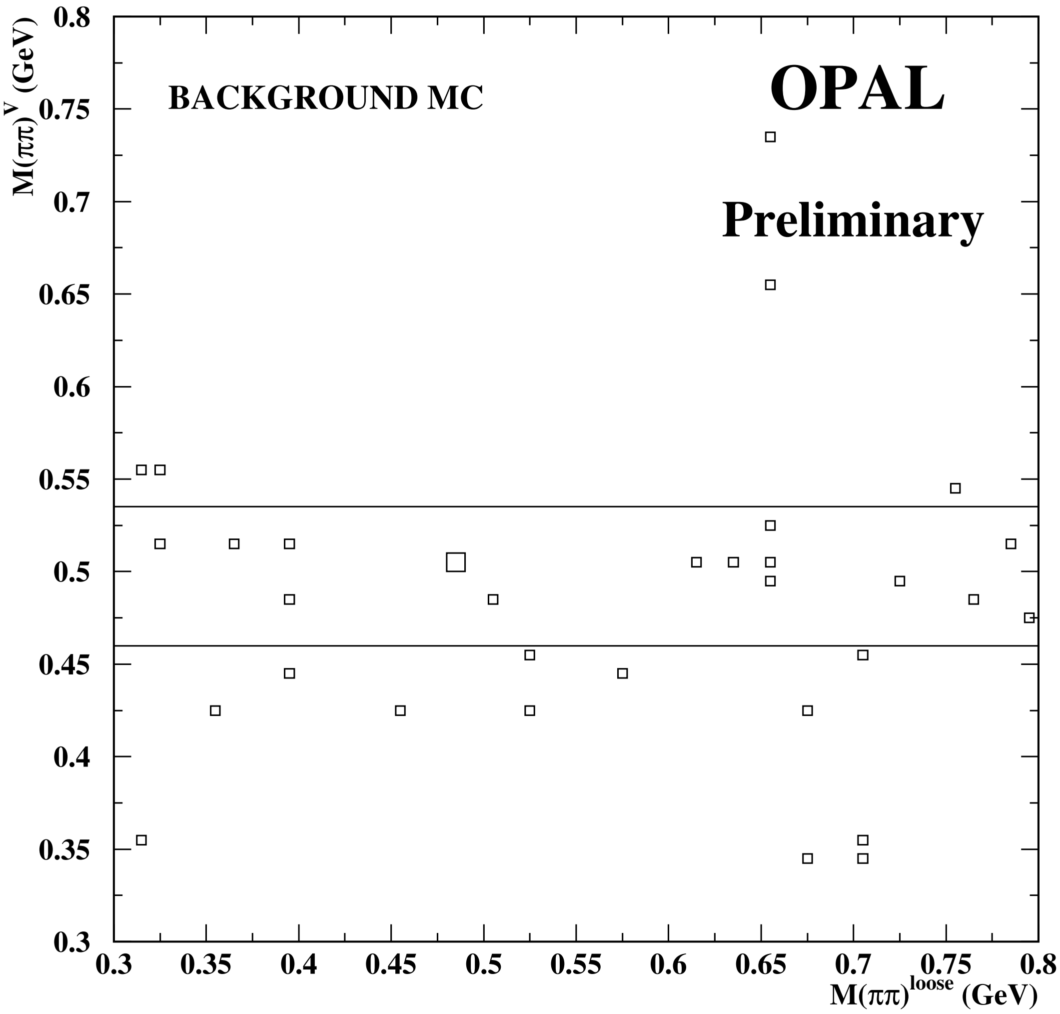
BACKGROUND MC
OPAL
Preliminary
0.8
0.75
0.7
0.65
0.6
0.55
0.5
0.45
0.4
0.35
0.3
M(ππ)^V (GeV)
0.3 0.35 0.4 0.45 0.5 0.55 0.6 0.65 0.7 0.75 0.8
M(ππ)^loose (GeV)

Figure 4